Photoinduced surface topography of nematic elastomers: a Green function approach

2008 J. Phys.: Condens. Matter 20 285107

(http://iopscience.iop.org/0953-8984/20/28/285107)

IOP Publishing Journal of Physics: Condensed Matter

J. Phys.: Condens. Matter **20** (2008) 285107 (9pp) doi:10.1088/0953-8984/20/28/285107

Photoinduced surface topography of nematic elastomers: a Green function approach

H T Chen and L H He[1]

CAS Key Laboratory of Mechanical Behavior and Design of Materials, University of Science and Technology of China, Hefei, Anhui 230026, People's Republic of China

E-mail: lhhe@ustc.edu.cn

Received 31 January 2008
Published 13 June 2008
Online at stacks.iop.org/JPhysCM/20/285107

Abstract

This paper studies photoinduced surface deformation of nematic elastomers containing azobenzene molecules. In the framework of a phenomenological model, a unified approach based on the Green function technique is proposed to predict the resulting surface topographies. The orientation of the nematic axis and the pattern of illumination can be arbitrary, and the calculation of the surface profile is finally reduced to the estimation of certain volume integrals. To demonstrate the application and to show the efficiency of the approach, two numerical examples are given. We expect that the present work can provide useful informative traces for creating desired surface topographies.

1. Introduction

Nematic elastomers possessing uniaxial orientational order can be synthesized by incorporating rod-like mesogenic groups into the strands of cross-linked polymer networks. The variation in the degree of alignment of mesogenic rods can deform the whole network [1]. When heated above the nematic–isotropic transition temperature, a shape change as high as 500% of such an elastomer can be observed [2]. Effectively, similar spontaneous deformation of nematic elastomers can also be achieved optically if the mesogenic groups are replaced by rod-like azobenzene derivatives [3–5]. Upon absorbing photons at suitable wavelengths, the azobenzene molecules suffer photoisomerization and change from the rod-like *trans*-state to the strongly kinked *cis*-state. This disrupts the nematic order of the elastomer and results in a contraction along the nematic axis. The photoinduced deformation is large and reversible, and the timescales vary from less than 100 ms [6, 7] to 1–10 s [8]. With these properties, the nematic elastomers become attractive for engineering micro-optical mechanical systems [9–12].

The fascinating photomechanical behavior of the nematic elastomers has been studied extensively. Besides the polarization-dependent photoresponse [13, 14], of special interest are inhomogeneous deformations because they are closely relevant to the application of nematic elastomers as photoactuators. Even if the nematic elastomer is irradiated uniformly with unilateral intensity, the light penetrating the face will be attenuated exponentially. It is this inhomogeneity of light intensity that generates a gradient of photostrain and thus bends a thin nematic elastomer beam or film [15–17]. More complex is the situation when the nematic elastomer is non-uniformly illuminated, e.g. the incident light is localized as a spot. A photostrain is induced in the irradiated part but not anywhere else, leading to the formation of pits and bumps on the elastomer surface. Warner and Mahadevan [15] proposed a scaling analysis of pits and bumps induced by shining light in circular spots, and suggested its use as a writable structure in microfluidics, switchable reflector elements in projective displays, etc. The idea is quite analogous to that of inscribing surface relief gratings onto amorphous azobenzene polymers [18, 19]. Nonetheless, the microscopic scenario in the nematic elastomers is different in that an occasional cross-link between chains resists large-scale mass transport, and thus elastic distortion becomes a predominant concern. Recently, Wei and He [20] utilized the Hankel transformation to perform a detailed calculation of the surface deformation in response to an illumination in circular spots, where the nematic axis of the nematic elastomer is normal to the surface. By using Fourier transformation, He [21] also obtained an analytical

[1] Author to whom any correspondence should be addressed.

solution to the surface deformation of a nematic elastomer with an arbitrary orientation of the nematic axis under striped illumination. These studies show strong dependence of the photoinduced surface topography not only on the pattern of illumination and the orientation of the nematic axis, but also on the absolute size of the illuminated region. Therefore, to create a desired surface topography on a nematic elastomer, the correlations between these factors should be well understood.

The present work aims at the development of an efficient way to predict the photoinduced surface topographies of nematic elastomers. Since in a general case of illumination the surface deformation may be very complicated, the methods adopted in the previous studies [20, 21] are inadequate in calculating the resulting surface profile. In this paper, inspired by the concept of eigenstrain in the theory of elastic inclusion [22], we propose a unified approach based on the Green function technique. The new method applies in principle to an arbitrary geometry of illumination pattern and to an arbitrary orientation of the nematic axis. In any case the calculation of surface topography finally can be reduced to the numerical estimation of certain volume integrals. To illustrate the application, numerical results for two examples are demonstrated. It is expected that the present method may be used as a helpful tool that could provide an informative trace for the creation of desired surface topographies on nematic elastomers by irradiation.

2. Theoretical formulation

Sketched in figure 1 is a monodomain nematic elastomer irradiated by a normally incident beam, with an illumination pattern Ω formed on the surface. Since the penetrating depth of photons is tiny, we approximate the elastomer as a half-space, $x_3 < 0$, with the undeformed surface coinciding with the x_1–x_2 plane of the rectangular coordinate system. The orientation of the nematic axis of the nematic elastomer can be arbitrary and is characterized by two angles ϕ and θ, where ϕ is the angle between the nematic axis and the x_3 axis, and θ stands for the angle between the surface projection of the nematic axis and the x_1 axis. Denote the light intensity on the surface $x_3 = 0$ by $I\delta(x_1, x_2)$, where I is a constant having the dimension of light intensity and $\delta(x_1, x_2)$ is a dimensionless function characterizing the intensity distribution. Then, according to Beer's law, the intensity at a point (x_1, x_2, x_3) in the elastomer decays exponentially with distance from the surface and can be written as

$$I(x_1, x_2, x_3) = I\delta(x_1, x_2)\, \mathrm{e}^{x_3/d}, \tag{1}$$

with d being the characteristic attenuation length. In the low-illumination limit, the photostrain induced by the *trans–cis* isomerization is proportional to the local intensity [15, 21]. By assuming elastic incompressibility of the elastomer, the photostrain components along and normal to the nematic axis, $\varepsilon^*_\parallel$ and $\varepsilon^*_\perp$, are

$$\varepsilon^*_\parallel = -\alpha I\delta(x_1, x_2)\, \mathrm{e}^{x_3/d}, \qquad \varepsilon^*_\perp = \tfrac{1}{2}\alpha I\delta(x_1, x_2)\, \mathrm{e}^{x_3/d}, \tag{2}$$

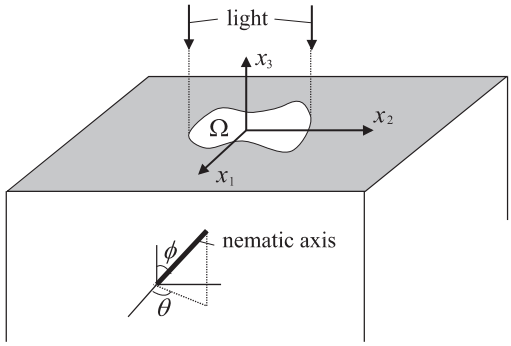

Figure 1. A nematic elastomer is illuminated by a light beam normally incident to the surface. The orientation of the nematic axis of the elastomer is arbitrary and characterized by two angles ϕ and θ.

with α being a phenomenological constant. Making use of coordinate transformation, the photostrain components referring to the (x_1, x_2, x_3) system, ε^*_{ij}, are obtained as

$$\varepsilon^*_{ij} = \lambda_{ij}\alpha I\delta(x_1, x_2)\, \mathrm{e}^{x_3/d}, \tag{3}$$

in which λ_{ij} are functions of θ and ϕ given by [21]

$$\begin{aligned}
\lambda_{11} &= \tfrac{1}{2}(1 - 3\cos^2\theta \sin^2\phi),\\
\lambda_{22} &= \tfrac{1}{2}(1 - 3\sin^2\theta \sin^2\phi),\\
\lambda_{33} &= \tfrac{1}{2}(1 - 3\cos^2\phi),\\
\lambda_{12} = \lambda_{21} &= -\tfrac{3}{2}\sin\theta\cos\theta\sin^2\phi,\\
\lambda_{13} = \lambda_{31} &= -\tfrac{3}{2}\cos\theta\sin\phi\cos\phi,\\
\lambda_{23} = \lambda_{32} &= -\tfrac{3}{2}\sin\theta\sin\phi\cos\phi.
\end{aligned} \tag{4}$$

Here and in the following, Latin indices range from 1 to 3, and repeated ones mean summation.

The photostrain components in (3) are position-dependent and incompatible. As a result, a spatially varying elastic strain must be produced which, being superposed to the photostrain, ensures the total strain is compatible. This is very analogous to the situation of the first-order transformation in solids for which the related problem of elastic deformation can be well treated via the concept of eigenstrain [22]. We will determine the total surface deformation of the nematic elastomer in the same way. For simplicity, we assume that the deformation is small and the elastomer is elastically isotropic and incompressible. Although approximate, these assumptions have been utilized in the previous studies [15, 17, 20, 21] to extract the main features of the problem while keeping the analysis as simple as possible. To start, we denote the displacement, strain and the stress in the elastomer by u_i, ε_{ij} and σ_{ij}, respectively. The incompressibility condition is expressed by $\partial u_k/\partial x_k = 0$, the strain–displacement relation is $\varepsilon_{ij} = (\partial u_i/\partial x_j + \partial u_j/\partial x_i)/2$ and the stress–strain relation is given by

$$\sigma_{ij} = -p\delta_{ij} + 2\mu\left(\varepsilon_{ij} - \varepsilon^*_{ij}\right), \tag{5}$$

where p is the average hydrostatical pressure, δ_{ij} refers to the Kronecker delta and μ denotes the shear modulus. In

the absence of body force, the stress satisfies the equilibrium equation $\partial\sigma_{ij}/\partial x_j = 0$. Thus, by supplying the associated boundary conditions $\sigma_{i3} = 0$ on the surface $x_3 = 0$, the deformation of the elastomer under a special illumination pattern can be determined in principle by solving the corresponding boundary value problem.

The present paper pursuits a unified approach for analyzing the photoinduced surface topography by using the technique of the Green function. In fact, the stress in (5) can be separated into two parts: one is $\sigma'_{ij} = -p\delta_{ij} + 2\mu\varepsilon_{ij}$, which corresponds to the stress in the situation that there is no photostrain, and the other is $-2\mu\varepsilon^*_{ij}$. Then the equilibrium equation becomes $\partial\sigma'_{ij}/\partial x_j - 2\mu\partial\varepsilon^*_{ij}/\partial x_j = 0$ and we can see that the role of the term $-2\mu\partial\varepsilon^*_{ij}/\partial x_j$ is equivalent to the action of a body force. In this case, by making use of the Green function tensor $G_{ij}(x_1 - x'_1, x_2 - x'_2, -x'_3)$, the surface displacement of the elastomer can be expressed formally by

$$u_i(x_1, x_2, 0) = -2\mu \int_{-\infty}^{0}\int_{-\infty}^{\infty}\int_{-\infty}^{\infty} G_{ij}(x_1 - x'_1, x_2 - x'_2, -x'_3) \times \frac{\partial\varepsilon^*_{jk}}{\partial x'_k}\,\mathrm{d}x'_1\,\mathrm{d}x'_2\,\mathrm{d}x'_3. \tag{6}$$

Here the Green function tensor $G_{ij}(x_1 - x'_1, x_2 - x'_2, -x'_3)$ defines the fundamental solution to the x_i component of the surface displacement at the point $(x_1, x_2, 0)$ induced by a concentrated unit force applied at the point (x'_1, x'_2, x'_3) within the elastomer along the x_j direction. Since the Green function for an elastically compressible half-space is available (see, e.g., [22]), the components of the Green function tensor related to our problem of an incompressible half-space are derivable by simply setting the Poisson's ratio as $1/2$. The results are

$$\begin{aligned} G_{31}(x_1 - x'_1, x_2 - x'_2, -x'_3) &= -\frac{(x_1 - x'_1)x'_3}{4\pi\mu R^3}, \\ G_{32}(x_1 - x'_1, x_2 - x'_2, -x'_3) &= -\frac{(x_2 - x'_2)x'_3}{4\pi\mu R^3}, \\ G_{33}(x_1 - x'_1, x_2 - x'_2, -x'_3) &= \frac{R^2 + x'^2_3}{4\pi\mu R^3}, \end{aligned} \tag{7}$$

with R being the distance between a point $(x_1, x_2, 0)$ on the surface and a point (x'_1, x'_2, x'_3) in the interior of the nematic elastomer, defined by

$$R = \sqrt{(x_1 - x'_1)^2 + (x_2 - x'_2)^2 + x'^2_3}. \tag{8}$$

The surface profile of the deformed elastomer is described by the position vector $\mathbf{r} = [x_i + u_i(x_1, x_2, 0)]\mathbf{e}_i$, where $\mathbf{e}_i$ stands for the base vector of x_i. In view of the smallness of the deformation in the low-illumination limit, we can approximate the position vector by $\mathbf{r} = x_1\mathbf{e}_1 + x_2\mathbf{e}_2 + u_3(x_1, x_2, 0)\mathbf{e}_3$, namely, only the normal component of the surface displacement contributes to the profile. Integrating (6) by parts and using (7), we arrive at

$$u_3(x_1, x_2, 0) = 2\mu \int_{-\infty}^{0}\int_{-\infty}^{\infty}\int_{-\infty}^{\infty} \varepsilon^*_{jk}\frac{\partial}{\partial x'_k} \times G_{3j}(x_1 - x'_1, x_2 - x'_2, -x'_3)\,\mathrm{d}x'_1\,\mathrm{d}x'_2\,\mathrm{d}x'_3. \tag{9}$$

Accordingly, the normal component of the surface displacement can be calculated. As the light has been assumed to be normally incident to the elastomer surface, the integral domain is effectively a cylinder with the cross section exactly identical to the illumination pattern on the surface. Obviously, the photoinduced topography of the surface depends not only on the geometry of the illumination pattern but also on the orientation of the nematic axis. For convenience of use, we give the derivatives of the Green function components with respect to x'_k as follows:

$$\begin{aligned} \frac{\partial G_{31}}{\partial x'_1} &= \frac{[R^2 - 3(x_1 - x'_1)^2]x'_3}{4\pi\mu R^5}, \\ \frac{\partial G_{31}}{\partial x'_2} = \frac{\partial G_{32}}{\partial x'_1} &= -\frac{3(x_1 - x'_1)(x_2 - x'_2)x'_3}{4\pi\mu R^5}, \\ \frac{\partial G_{31}}{\partial x'_3} &= -\frac{(x_1 - x'_1)(R^2 - 3x'^2_3)}{4\pi\mu R^5}, \\ \frac{\partial G_{32}}{\partial x'_2} &= \frac{[R^2 - 3(x_2 - x'_2)^2]x'_3}{4\pi\mu R^5}, \\ \frac{\partial G_{32}}{\partial x'_3} &= -\frac{(x_2 - x'_2)(R^2 - 3x'^2_3)}{4\pi\mu R^5}, \\ \frac{\partial G_{33}}{\partial x'_1} &= \frac{(x_1 - x'_1)(R^2 + 3x'^2_3)}{4\pi\mu R^5}, \\ \frac{\partial G_{33}}{\partial x'_2} &= \frac{(x_2 - x'_2)(R^2 + 3x'^2_3)}{4\pi\mu R^5}, \\ \frac{\partial G_{33}}{\partial x'_3} &= \frac{x'_3(R^2 - 3x'^2_3)}{4\pi\mu R^5}. \end{aligned} \tag{10}$$

3. Illustrative examples

To illustrate the application of this work, we will consider two typical examples. The first example is the photoinduced surface topography of a nematic elastomer under striped illumination. The problem has an analytical solution and the related phenomena have also been discussed in detail [21]. We will compare our numerical results based on equation (9) with the corresponding predictions of the analytical solution so as to validate the present approach. The second example deals with the calculation of the surface topography of an elastomer under illumination in an annular pattern. A special case when the nematic axis is normal to the elastomer surface has been studied previously [20]. However, our attention here is focused on a much more complicated situation, that the nematic axis can be arbitrarily oriented. The objective is to show the efficiency of the proposed method utilizing the Green function technique. In all the examples the coordinates and the normal component of surface displacement are normalized as

$$\begin{aligned} X_i &= \frac{x_i}{d}, \qquad y_i = \frac{x'_i}{d}, \\ U_3(X_1, X_2) &= \frac{4\pi}{\alpha I d}u_3(x_1, x_2, 0). \end{aligned} \tag{11}$$

3.1. The case of striped illumination

Suppose that the elastomer is irradiated so that the illumination pattern is a stripe, with the half-width a, parallel to the x_2 axis (figure 2). This is equivalent to setting the function $\delta(x_1, x_2)$ in (1) as $\delta(x_1, x_2) = H(a - |x_1|)$, where $H(x)$ stands for the step function. In this case the integration domain of (9) is characterized by $-a \leqslant x_1' \leqslant a$, $-\infty < x_2' < \infty$ and $-\infty < x_3' \leqslant 0$. Making use of (10), we have

$$\begin{aligned}
&\int_{-\infty}^{\infty} \frac{\partial G_{31}}{\partial x_1'}(x_1 - x_1', x_2 - x_2', -x_3')\,\mathrm{d}x_2' \\
&= -\frac{\left[(x_1 - x_1')^2 - x_3'^2\right] x_3'}{2\pi\mu\left[(x_1 - x_1')^2 + x_3'^2\right]^2}, \\
&\int_{-\infty}^{\infty} \frac{\partial G_{31}}{\partial x_3'}(x_1 - x_1', x_2 - x_2', -x_3')\,\mathrm{d}x_2' \\
&= -\frac{(x_1 - x_1')\left[(x_1 - x_1')^2 - x_3'^2\right]}{2\pi\mu\left[(x_1 - x_1')^2 + x_3'^2\right]^2}, \\
&\int_{-\infty}^{\infty} \frac{\partial G_{33}}{\partial x_1'}(x_1 - x_1', x_2 - x_2', -x_3')\,\mathrm{d}x_2' \\
&= \frac{(x_1 - x_1')\left[(x_1 - x_1')^2 + 3x_3'^2\right]}{2\pi\mu\left[(x_1 - x_1')^2 + x_3'^2\right]^2}, \\
&\int_{-\infty}^{\infty} \frac{\partial G_{33}}{\partial x_3'}(x_1 - x_1', x_2 - x_2', -x_3')\,\mathrm{d}x_2' \\
&= \frac{x_3'\left[(x_1 - x_1')^2 - x_3'^2\right]}{2\pi\mu\left[(x_1 - x_1')^2 + x_3'^2\right]^2}.
\end{aligned} \tag{12}$$

Therefore, by invoking (3) and (10)–(12), it is inferred from (9) that the dimensionless component of surface displacement is reduced to

$$\begin{aligned}
U_3(X_1, X_2) = 4\int_{-\infty}^{0}\int_{-s}^{s} &\left[(\lambda_{33} - \lambda_{11})(\rho^2 - 2y_3^2)\right. \\
&\left. + 4\lambda_{13}(X_1 - y_1)y_3\right] y_3\rho^{-4}\,\mathrm{e}^{y_3}\,\mathrm{d}y_1\,\mathrm{d}y_3,
\end{aligned} \tag{13}$$

where $\rho = \sqrt{(X_1 - y_1)^2 + y_3^2}$ and $s = a/d$ is the normalized half-width of the stripe. Clearly, the result is independent of the coordinate in the direction parallel to the stripe.

The normalized surface displacement in (13) can be calculated numerically. In the computation, the Simpson integral form is used for y_1 with the step length 0.02, while the rectangular integral form is adopted for y_3 with the step length 0.02. Figures 3(a) and (b) show the surface topographies in the cases of $(\phi, \theta) = (\pi/2, 0)$ and $(\phi, \theta) = (\pi/4, 0)$, respectively, where the normalized stripe widths are both taken as $s = 5$. The results are fully consistent with those given by the recent analytical solution [21]. In fact, we have also examined dimensionless surface displacements for different stripe widths and nematic axis orientations, and found that the results are almost the same as the predictions of the analytical solution. Thus, without further discussion, we conclude that the present approach based on the Green function technique can recover the results of the analytical solution.

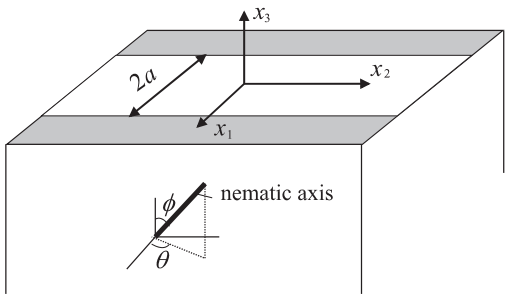

Figure 2. Sketch of the nematic elastomer under striped illumination. The illumination pattern on the surface is a stripe parallel to the x_2 axis, with the half-width a.

3.2. The case of annular illumination

As the second example, we consider the situation that the elastomer is illuminated in an annular pattern with the inner radius r_1 and outer radius r_2 (figure 4). Since the illumination pattern is axisymmetric, we can assume, without loss of any generality, that the nematic axis of the elastomer is in the plane perpendicular to the x_2 axis, i.e. $\theta = 0$. In addition, for brevity of the discussion, only three typical values of the angle ϕ are taken into account: $\phi = 0, \pi/4$ and $\pi/2$. To obtain the normal component of surface displacement from (9), it is convenient to introduce the transformation of $x_1'/d = r\cos\varphi$, $x_2'/d = r\sin\varphi$ and $x_3'/d = z$. In this case the integration domain becomes $r_1/d \leqslant r \leqslant r_2/d$, $0 \leqslant \varphi \leqslant 2\pi$ and $-\infty < z \leqslant 0$, and the normalized form of the surface displacement is

$$U_3(X_1, X_2) = 3\int_{-\infty}^{0}\int_{0}^{2\pi}\int_{r_1/d}^{r_2/d} \frac{rzf(r, \varphi, z)}{\hat{R}^5}\,\mathrm{e}^z\,\mathrm{d}r\,\mathrm{d}\varphi\,\mathrm{d}z, \tag{14}$$

where $\hat{R} = \sqrt{(X_1 - r\cos\varphi)^2 + (X_2 - r\sin\varphi)^2 + X_3'^2}$ and the function $f(r, \varphi, z)$ is defined by

$$\begin{aligned}
&f(r, \varphi, z) \\
&= \begin{cases}
3z^2 - \hat{R}^2, & \text{for } \phi = 0, \\
\frac{1}{2}[\hat{R}^2 - 3(X_2 - r\sin\varphi)^2] & \\
\quad - 3(X_1 - r\cos\varphi)z, & \text{for } \phi = \pi/4, \\
\hat{R}^2 - 3(X_1 - r\cos\varphi)^2, & \text{for } \phi = \pi/2.
\end{cases}
\end{aligned} \tag{15}$$

In the numerical computation, both the precision and computational efficiency are important. We have tested different step lengths and found that the truncation error is more sensitive to the step length of r than that of φ and z. Thus, we adopt the Simpson integral form for r, and the rectangular integral form for φ and z. When the step lengths of r, φ and z are chosen as 0.02, 0.01 and 0.08, respectively, the maximal truncation error is less than 1% in comparison with the results for shorter step lengths. In light of the convergence of the integrals, it is believed that the step lengths of 0.2, 01 and 0.8 for r, φ and z, respectively, are short enough to ensure the precision of the integrals. The lower limit of z is taken as -20 for the above reason.

We first examine the case of $\phi = 0$, i.e. the nematic axis is normal to the elastomer surface. The ratio $s = r_1/r_2$ is introduced to describe the relative size of the inner radius in

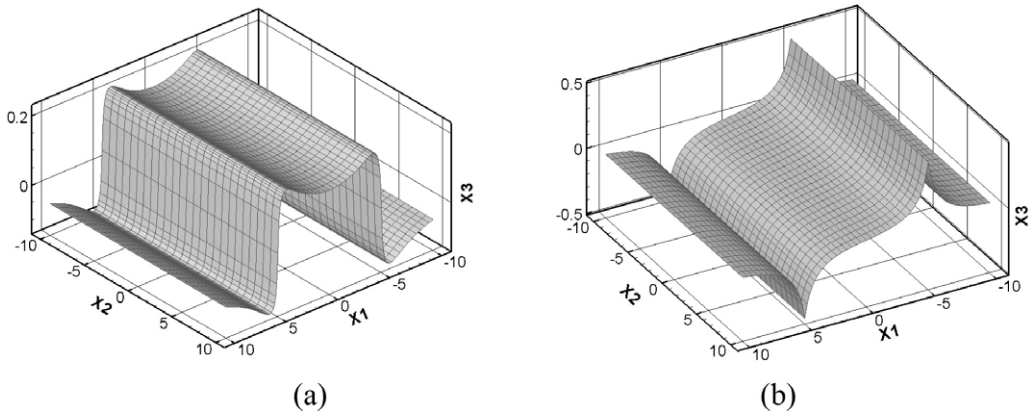

Figure 3. Schematic illustration of the surface topographies under striped illumination: (a) for the nematic orientation of $\phi = \pi/2$ and $\theta = 0$, the profile of the cross section is 'M'-shaped; (b) for the nematic orientation of $\phi = \pi/4$ and $\theta = 0$, the profile of the cross section is 'N'-shaped. In both cases the normalized half-width of the stripe is taken as $r = 5$ and the scales in the three directions are normalized by $X_1 = x_1/d$, $X_2 = x_2/d$ and $X_3 = 4\pi u_3/\alpha I d$.

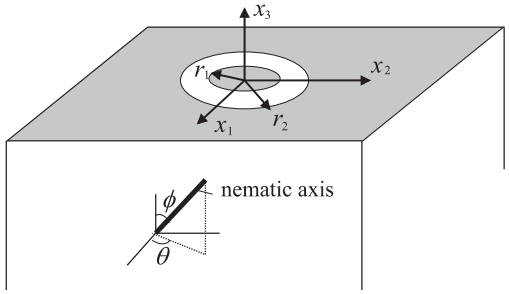

Figure 4. Sketch of the nematic elastomer under annular illumination. The illumination pattern is an annulus with the inner and outer radii r_1 and r_2, respectively.

comparison with the outer. Clearly, $s = 0.0$ means that the annular pattern is reduced to a circular spot. Figure 5 illustrates the surface topographies for fixed outer radius of $r_2 = d$ but varying inner radius. All the topographies are axisymmetric. As seen from figure 5(a), if $s = 0.0$, the illuminated area caves in, forming a single pit with the lowest point at the center. This is consistent with the previous prediction by using the Hankel transformation [20]. If $s = 0.2$, the topography is an annular pit with a small protuberant cone at the center (figure 5(b)). The formation of the small cone is due to that the material there is unexposed. Analogous surface topography can be observed if $s = 0.5$, except the cone appearing in the bottom of the pit becomes larger (figure 5(c)). Figure 6 illustrates the photoinduced surface topographies when the outer radius of the illuminated pattern is fixed as $r_2 = 5d$, where figure 6(a) is shown upside-down for a clearer visualization. For $s = 0.0$, 0.2 and 0.5, the topographies, given respectively in figures 6(a)–(c), are globally similar to the corresponding ones in figure 5. The differences are small and appear only in some local regions. For example, different from that in figure 5(a), the bottom of the pit in figure 6(a) mounds slightly and the boundary of the illuminated region reaches the maximal height. The phenomenon has been attributed to the elastic confinement from the unexposed surrounding material [20].

Next, when $\phi = \pi/4$, the nematic axis is neither normal nor parallel to the elastomer surface. Figures 7 and 8 depict the surface topographies for $r_2 = d$ and $5d$, respectively. Since a much sharper shape transition occurs near the boundary region of the illumination pattern, the density of data points has been enhanced in some locations (the darker regions) in figure 8. At the same radius ratio s, the surface profiles in both figures possess similar features. For example, at $s = 0.0$, the illuminated elastomer protrudes out in the region $x_1 < 0$ while it caves in at the position of $x_1 > 0$, and thus there is a sharp transition between these two regions. Again, at $s = 0.2$, a small protuberant cone of the unexposed elastomer appears at the center of the illuminated area. This is also the case at $s = 0.5$.

Finally, when $\phi = \pi/2$, the nematic axis of the elastomer is parallel to the surface. The topographies for $r_2 = d$ and $5d$ are plotted in figures 9 and 10, respectively, where the results of different radius ratios are compared as well. At $s = 0.0$, the illuminated material contracts in the nematic direction and thus protrudes out to form a saddle. The top of the saddle is rounded in the case of $r_2 = d$ (figure 9(a)), while it caves in slightly in the case of $r_2 = 5d$ (figure 10(a)). At $s = 0.2$, the unexposed surface in the central region becomes lower than the surface of the illuminated annular region. Consequently, for both $r_2 = d$ and $5d$, the resulting topographies look like saddles with an opening mouth at the center (figures 9(b) and 10(b)). If the ratio s increases to 0.5, the saddles and the opening mouths enlarge as well, as seen from figures 9(c) and 10(c). This implies that the photoinduced surface topography is dependent not only the nematic orientation but also on the size and shape of the illumination pattern.

4. Conclusions

By introducing the Green function technique, a route to predict the photoinduced surface topography of nematic elastomers containing photosensitive azobenzene molecules is proposed. The approach is quite general as it applies to arbitrary illumination patterns and arbitrary orientations of the nematic

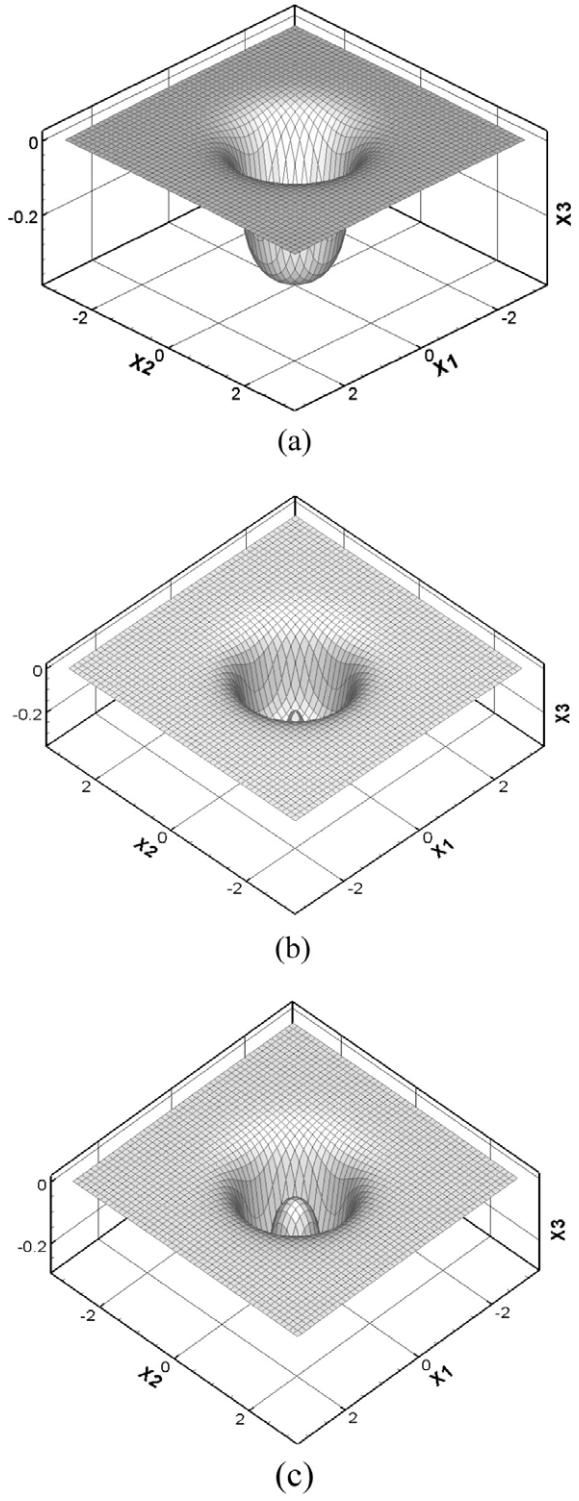

Figure 5. Photoinduced surface topographies under annular illumination for $r_2 = d$, $\phi = 0$ and (a) $s = 0.0$, (b) $s = 0.2$ and (c) $s = 0.5$, respectively. The scales in the three directions are normalized by $X_1 = x_1/d$, $X_2 = x_2/d$ and $X_3 = 4\pi u_3/\alpha I d$.

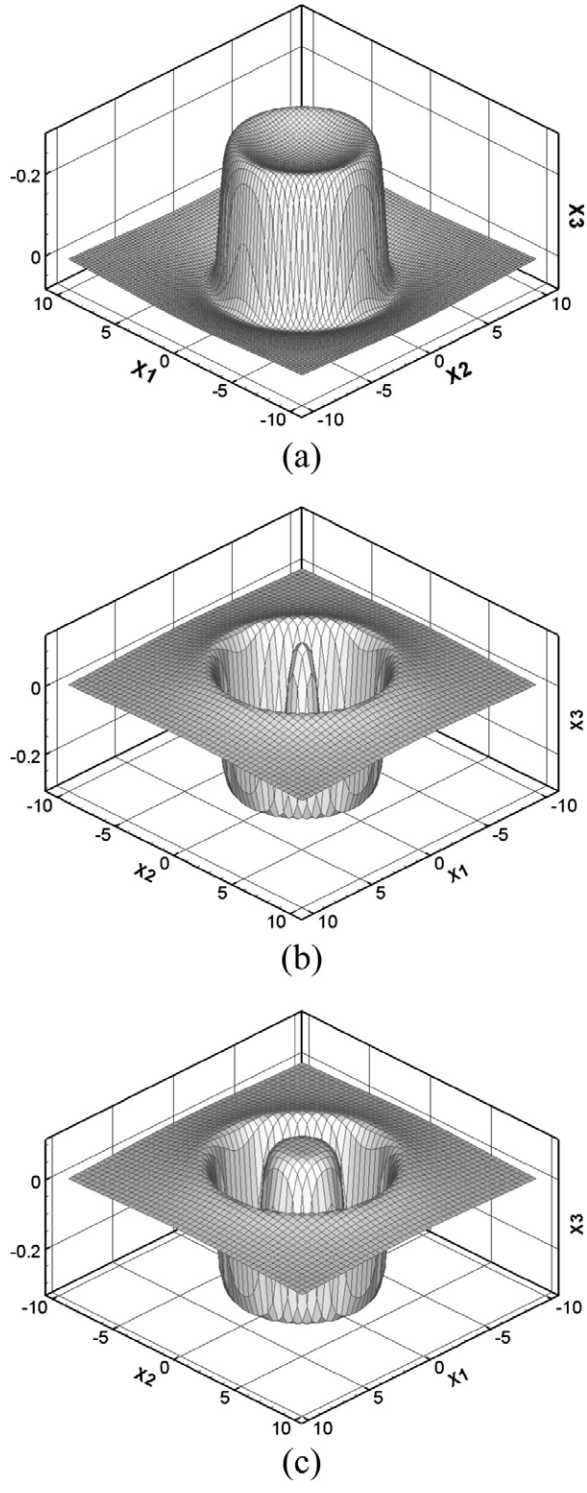

Figure 6. Photoinduced surface topographies under annular illumination for $r_2 = 5d$, $\phi = 0$ and (a) $s = 0.0$, (b) $s = 0.2$ and (c) $s = 0.5$, respectively. Figure (a) is shown upside-down to get a clearer visualization. The scales in the three directions are normalized by $X_1 = x_1/d$, $X_2 = x_2/d$ and $X_3 = 4\pi u_3/\alpha I d$.

axis. In any case the procedure is reduced to estimating certain integrals defined on appropriate domains. To demonstrate the application of the present method, two numerical examples are given. The results are in excellent agreement with the previous analytical solution in some special cases, and reveal the large complication of the dependence of the surface topography on such factors as the size and shape of the illumination pattern as well as the orientation of the nematic axis. Certainly,

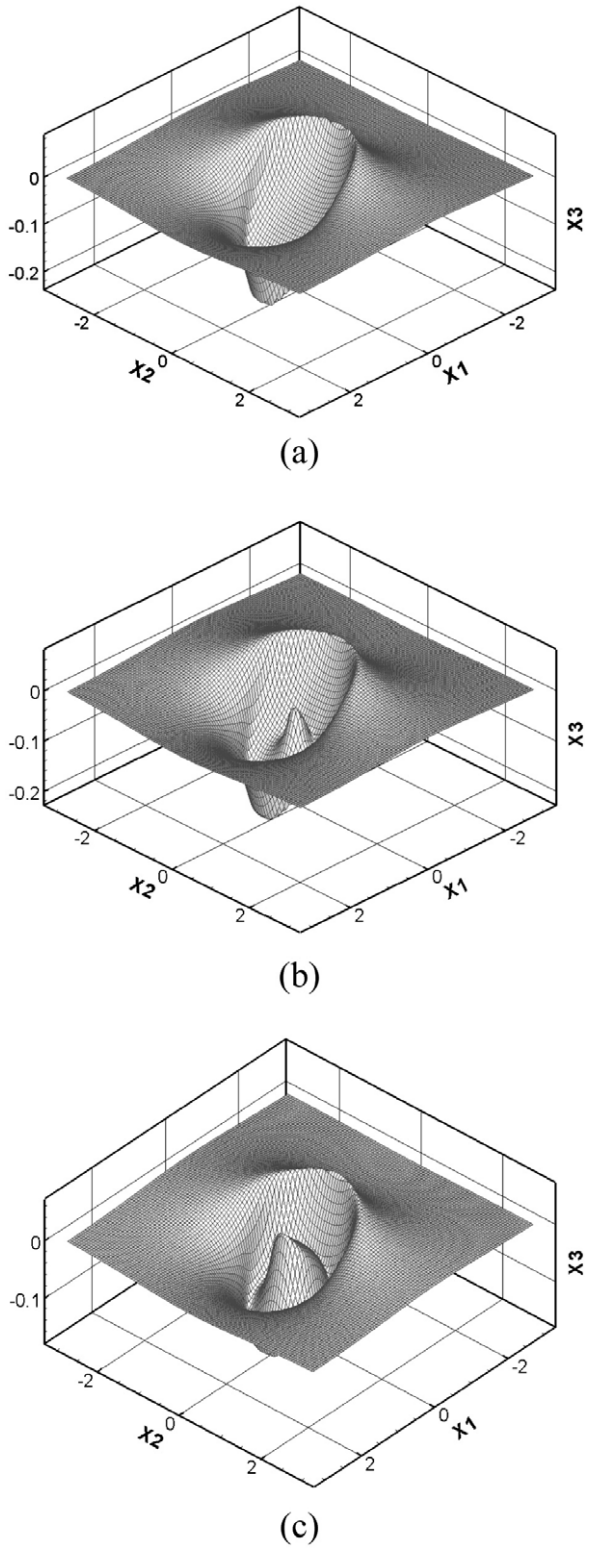

Figure 7. Photoinduced surface topographies under annular illumination for $r_2 = d$, $\phi = \pi/4$ and (a) $s = 0.0$, (b) $s = 0.2$ and (c) $s = 0.5$, respectively. The scales in the three directions are normalized by $X_1 = x_1/d$, $X_2 = x_2/d$ and $X_3 = 4\pi u_3/\alpha I d$.

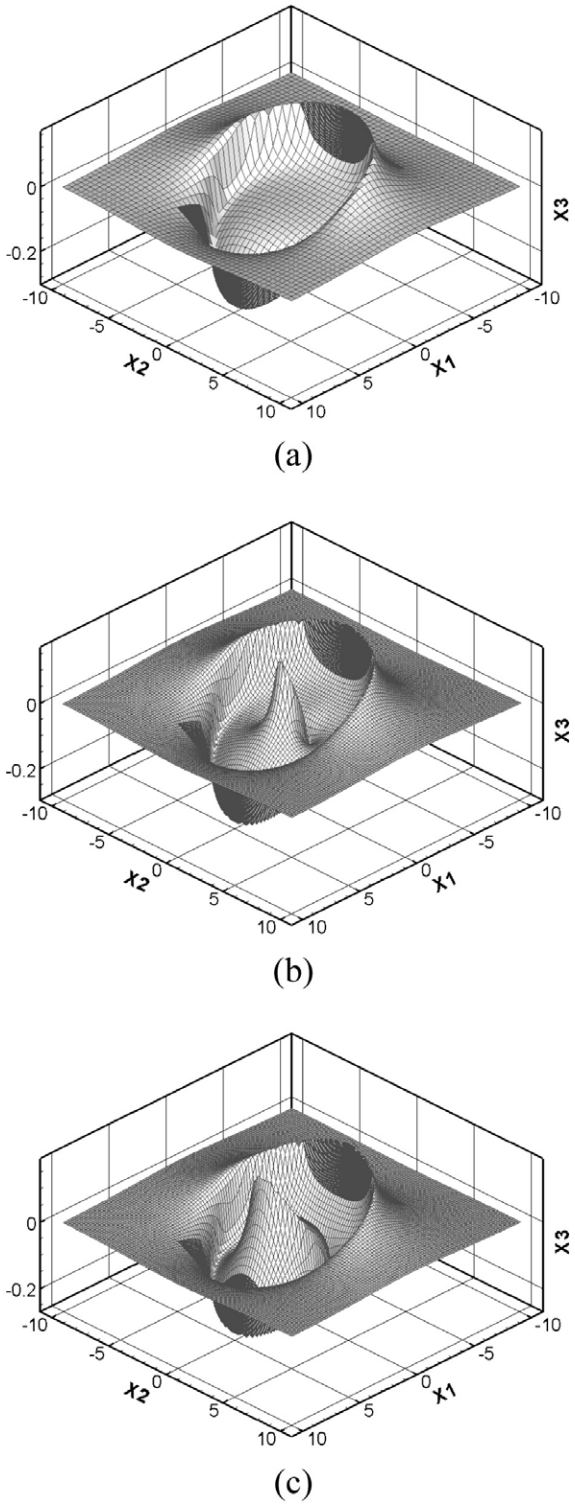

Figure 8. Photoinduced surface topographies under annular illumination for $r_2 = 5d$, $\phi = \pi/4$ and (a) $s = 0.0$, (b) $s = 0.2$ and (c) $s = 0.5$, respectively. The darker regions mean the locations where the density of data points are enhanced. The scales in the three directions are normalized by $X_1 = x_1/d$, $X_2 = x_2/d$ and $X_3 = 4\pi u_3/\alpha I d$.

the approach developed in this paper is phenomenological in nature, and some important effects such as the isomerization dynamics of azobenzene molecules and the elastic anisotropy and large deformation of the elastomers were not considered. Incorporation of these aspects into the model is undoubtedly of theoretical and practical importance, and will be the main

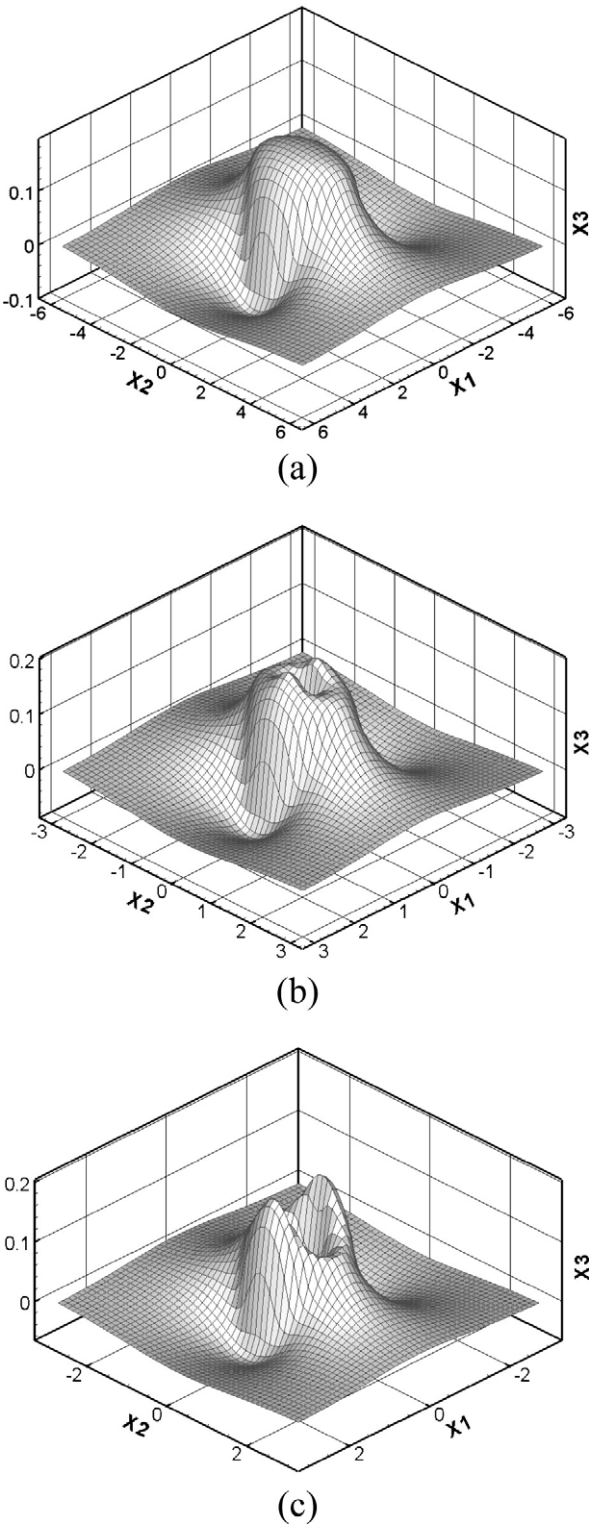

Figure 9. Photoinduced surface topographies under annular illumination for $r_2 = d$, $\phi = \pi/2$ and (a) $s = 0.0$, (b) $s = 0.2$ and (c) $s = 0.5$, respectively. The scales in the three directions are normalized by $X_1 = x_1/d$, $X_2 = x_2/d$ and $X_3 = 4\pi u_3/\alpha I d$.

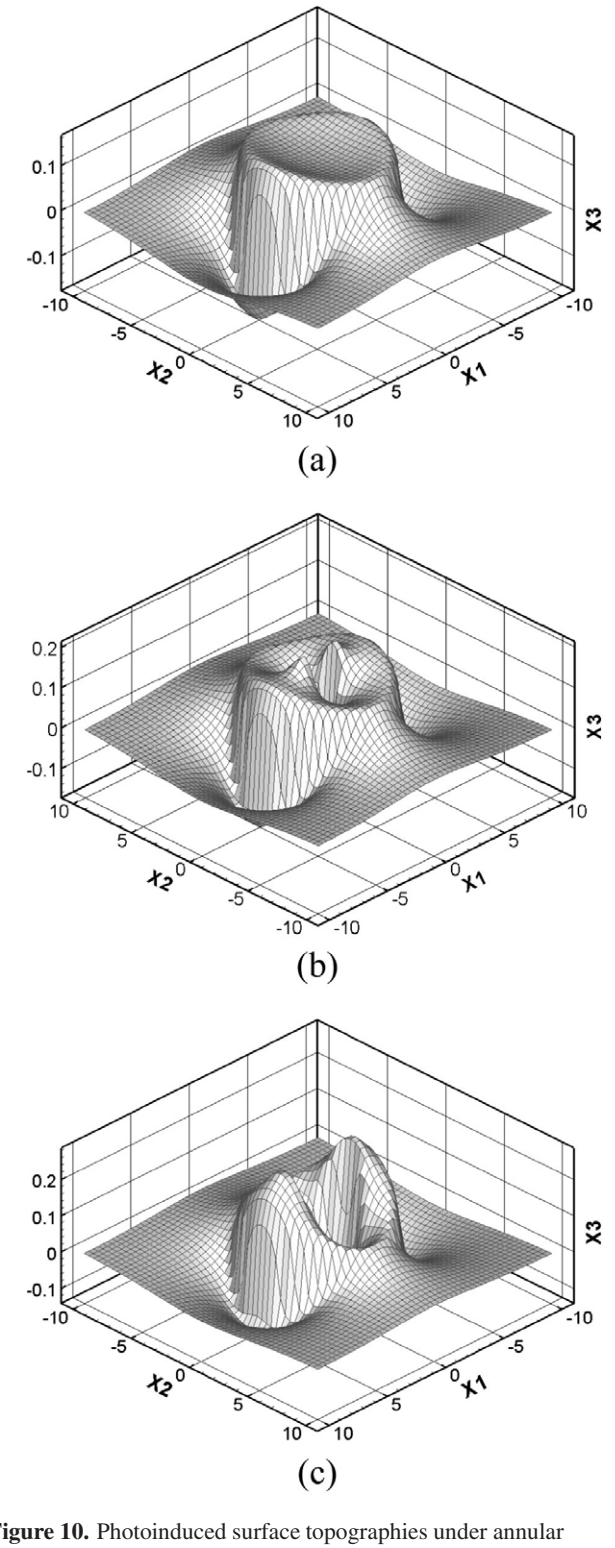

Figure 10. Photoinduced surface topographies under annular illumination for $r_2 = 5d$, $\phi = \pi/2$ and (a) $s = 0.0$, (b) $s = 0.2$ and (c) $s = 0.5$, respectively. The scales in the three directions are normalized by $X_1 = x_1/d$, $X_2 = x_2/d$ and $X_3 = 4\pi u_3/\alpha I d$.

content of a future study. In spite of these, we believe that the present work may provide a useful tool to search for some informative trace, at least in a qualitative sense, for creating a desired surface topography in the optical way.

Acknowledgments

This work is supported by the Chinese National Natural Science Foundation (grant nos. 10472109, 10625212), the Basic Research Program of China (grant no. 2006CB300404)

and the PhD Programs Foundation of Ministry of Education of China (grant no. 20060358044).

References

[1] Warner M and Terentjev E M 2003 *Liquid Crystal Elastomers* (Oxford: Clarendon)
[2] Ahir S V, Tajbakhsh A R and Terentjev E M 2006 *Adv. Funct. Mater.* **16** 556
[3] Hinkelmann F, Nishikawa E, Pereira G G and Warner M 2001 *Phys. Rev. Lett.* **87** 015501
[4] Hogan P M, Tajbakhsh A R and Terentjev E M 2002 *Phys. Rev.* E **65** 041720
[5] Cviklinski J, Tajbakhsh A R and Terentjev E M 2002 *Eur. Phys. J.* E **9** 427
[6] Ikeda T 2003 *J. Mater. Chem.* **13** 2037
[7] Camacho-Lopez M, Finkelmann H, Palffy-Muhoray P and Shelley M 2004 *Nat. Mater.* **3** 307
[8] Yu Y, Nakano M and Ikeda T 2003 *Nature* **425** 145
[9] Ciuchi F, Mazzulla A and Cipparrone G 2002 *J. Opt. Soc. Am.* B **19** 2531
[10] Tabiryan N, Serak S, Dai X and Bunning T 2005 *Opt. Express* **13** 7442
[11] Kondo M, Yu Y and Ikeda T 2006 *Angew. Chem.* **45** 1378
[12] Gorkhali S P, Cloutier S G and Crawford G P 2006 *Appl. Phys. Lett.* **88** 251113
[13] Corbett D and Warner M 2006 *Phys. Rev. Lett.* **96** 237802
[14] Harvey C L M and Terentjev E M 2007 *Eur. Phys. J.* E **23** 185
[15] Warner M and Mahadevan L 2004 *Phys. Rev. Lett.* **92** 134302
[16] Corbett D and Warner M 2007 *Phys. Rev. Lett.* **99** 174302
[17] Dunn M L 2007 *J. Appl. Phys.* **102** 013506
[18] Rochon P, Batalla E and Natansohn A 1995 *Appl. Phys. Lett.* **66** 136
[19] Kim D Y, Li L, Jiang X L, Shivshankar V, Kumar J and Tripathy S K 1995 *Macromolecules* **28** 8835
[20] Wei Z Y and He L H 2006 *J. Chem. Phys.* **124** 064708
[21] He L H 2007 *Phys. Rev.* E **75** 041702
[22] Mura T 1987 *Micromechanics of Defects in Solids* (Dordrecht: Martinus Nijhoff)